Astronomy & Astrophysics manuscript no. 12477ms
November 7, 2009

High-dispersion infrared spectroscopic observations of comet 8P/Tuttle with VLT/CRIRES⋆

H. Kobayashi[1], D. Bockelée-Morvan[2], H. Kawakita[1], N. Dello Russo[3], E. Jehin[4], J. Manfroid[4], A. Smette[5], D. Hutsemékers[4], J. Stüwe[6], M. Weiler[7], C. Arpigny[4], N. Biver[2], A. Cochran[8], J. Crovisier[2], P. Magain[4], H. Sana[5], R. Schulz[9], R. J. Vervack[3], H. Weaver[3], and J. -M. Zucconi[10,⋆⋆]

(Affiliations can be found after the references)

Received **** **, 2009; accepted **** **, 2009

ABSTRACT

We report on the composition of the Halley-family comet (HFC) 8P/Tuttle investigated with high-dispersion near-infrared spectroscopic observations. The observations were carried out at the ESO VLT (Very Large Telescope) with the CRIRES instrument as part of a multi-wavelength observation campaign of 8P/Tuttle performed in late January and early February 2008. Radar observations suggested that 8P/Tuttle is a contact binary, and it was proposed that these components might be heterogeneous in chemistry. We determined mixing ratios of organic volatiles with respect to H_2O and found that mixing ratios were consistent with previous near infrared spectroscopic observations obtained in late December 2007 and in late January 2008. It has been suggested that because 8P/Tuttle is a contact binary, it might be chemically heterogeneous. However, we find no evidence for chemical heterogeneity within the nucleus of 8P/Tuttle. We also compared the mixing ratios of organic molecules in 8P/Tuttle with those of both other HFCs and long period comets (LPCs) and found that HCN, C_2H_2, and C_2H_6 are depleted whereas CH_4 and CH_3OH have normal abundances. This may indicate that 8P/Tuttle was formed in a different region of the early solar nebula than other HFCs and LPCs. We estimated the conversion efficiency from C_2H_2 to C_2H_6 by hydrogen addition reactions on cold grains by employing the $C_2H_6/(C_2H_6+C_2H_2)$ ratio. The $C_2H_6/(C_2H_6+C_2H_2)$ ratio in 8P/Tuttle is consistent with the ratios found in other HFCs and LPCs within the error bars. We also discuss the source of C_2 and CN based on our observations and conclude that the abundances of C_2H_2 and C_2H_6 are insufficient to explain the C_2 abundances in comet 8P/Tuttle and that the abundance of HCN is insufficient to explain the CN abundances in the comet, so at least one additional parent is needed for each species, as pointed out in previous study.

Key words. Comets: individual: 8P/Tuttle – Solar system: formation – Kuiper Belt

1. Introduction

Comets are remnants of planetesimals formed in the early solar nebula. Their nuclei consist of volatile ices and dust grains and are thought to preserve primordial information such as temperature, degree of ionization, and chemistry. Comet composition may also provide clues about the dynamical evolution of planetesimals in the early solar system. Comets are dynamically classified by their Tisserand invariants with respect to Jupiter (T_J): ecliptic comets ($T_J > 2$, here we call them Jupiter family comets: JFCs) and nearly isotropic comets (NICs, $T_J < 2$) (Levison, 1996). The NICs are further divided into two sub-classes: long period comets (LPCs, semi-major axis (a) $>$ 40 AU) and Halley-family comets (HFCs, a $<$ 40 AU) (Levison, 1996). The dynamical origin of LPCs is thought to be the Oort cloud whereas JFCs are thought to originate in the classical Kuiper Belt and/or the scattered disk. The dynamical origin of HFCs is unclear and still under debate. They were injected either into the inner part of the Oort cloud or into the outer part of the scattered disk (Duncan, 2008).

HFCs have long been studied by spectrophotometry at optical wavelengths (e.g., A'Hearn et al. 1995). Optical spectroscopic observations allow us to observe the daughter species produced by photo-dissociation of parent (or grandparent, etc.) species in the coma, e.g., H_2O, HCN, and C_2H_2. Strong vibrational and/or rotational transitions of parent species are observable in the near infrared and radio regions of the spectrum (Bockelée-Morvan et al. 2004). As an example, Biver et al. (2002) and Crovisier et al. (2008) reported the mixing ratios of parent molecules in four HFCs observed at radio wavelengths. In the near infrared region, DiSanti & Mumma (2008) summarized the mixing ratios of organic volatiles for two HFCs (153P/Ikeya-Zhang and 1P/Halley). Because of the small sample size, the chemistry of HFCs as a group is still not well-characterized.

Our scientific goal in the present work is to determine the relative production rates (mixing ratios) of organic volatiles in the HFC 8P/Tuttle by using high-dispersion spectroscopic observations in the near infrared spectral region. This project is part of a multi-wavelength study of 8P/Tuttle performed at the VLT (see Section 2). In the present paper, we will focus on observations taken with the CRIRES spectrometer. In section 3, we will derive rotational temperatures and mixing ratios of organic volatiles in comet 8P/Tuttle. Bonev et al. (2008) and Boehnhardt et al. (2008) also reported mixing ratios of organic volatiles in comet 8P/Tuttle from near infrared high-dispersion spectroscopic observations. We compare thses results with ours in Section 4.

To be cited as: A&A preprint doi http://dx.doi.org/10.1051/0004-6361/200912477

2. Observations and data reduction

Comet 8P/Tuttle was observed at multiple wavelengths using the ESO Very Large Telescope (VLT) located on Cerro Paranal in Chile. We observed this comet using UVES (Unit Telescope (UT) 2) on January 16, 28 and February 4, 2008, and FORS1 (UT2) and CRIRES (UT1), on January 28 and February 4, 2008. The V-band magnitudes of 8P/Tuttle were 7 – 8 in this period. Here we focus on the near-infrared high dispersion spectroscopic observations with CRIRES. The CRIRES (CRyogenic high-resolution InfraRed Echelle Spectrograph, Käufl et al. 2004) can achieve high resolving power ($\lambda/\Delta\lambda$ ∼100,000 with the slit width of 0.2", i.e., $\Delta\lambda \sim 0.03$ nm at 3000 nm). CRIRES records a single echelle order on a mosaic of four InSb Aladdin III arrays with 27 μm pixels. The mechanical gaps between 2 arrays correspond to about 280 pixels. The telescope was nodded between two different positions (A and B, separated by 15") in a dithering sequence of ABBA (position A (image "A1") → position B (image "B1") → position B (image "B2") → position A (image "A2")) with jittering (small random offset). We used two different wavelength settings on Jan. 28 (a setting #1 for H_2O, and a setting #2 for HCN and C_2H_2) and 3 settings on Feb. 4 (a setting #1′ for H_2O, a setting #3 for CH_4 and C_2H_6, and a setting #4 for CH_3OH). The wavelength coverage of each setting is given in Table 1. The slit widths were 0.2" and 1.0" for the comet and a flux standard star (30 Mon; spectral type: A0V), respectively. The slit length was 31" for both cases.

Data were processed using the Image Reduction and Analysis Facility (IRAF) software package distributed by NOAO. For each sequence of ABBA, we calculated (A1 – B1 – B2 + A2) to remove sky background emission. Wavelength calibration and re-sampling of spectra were performed by comparing measured sky background emission lines and modeled atmospheric radiance spectra. Since we also employed "jittering" along the slit (random small offsets at both A and B positions to avoid severe defects on the arrays), we spatially registered the spectra before combining them into a single two-dimensional spectrum (Figure 1). We extracted a one-dimensional (1-D) spectrum from an aperture [0.2" × ∼0.8"] centered on the nucleus.

The 1-D spectrum was flux calibrated as follows. The spectra of the standard star were compared with the synthesized stellar spectra (combined with the telluric absorption at a given airmass by the LBLRTM code, Clough et al. 1995) to evaluate the efficiency of both the telescope and the CRIRES instrument. The flux loss of the standard star at the slit (1.0" slit width) was estimated from the brightness spatial profile of the star along the slit. Since the spatial profile has a concentrated core and a wing part, we modeled the spatial profile as a linear combination of two 2-D Gaussian functions (one for the core and another for the wing part). The throughput of the slit was estimated based on this modeled profile. After that, we calibrated the cometary spectra based on the efficiencies determined for the standard star. Therefore, the telluric absorption was not corrected for the comet at this stage and this would be corrected for each emission line later. The difference in airmass between the comet and the standard star was taken into account by using the LBLRTM code.

The cometary continuum component (reflected sunlight) was modeled as a product of the smoothed continuum and the synthesized atmospheric transmittance calculated by the LBLRTM code. The continuum component was removed by using this modeled spectrum. The calibrated (but not corrected for the telluric absorption) cometary emission spectra are shown in Figure 2 and 3, and the detected emission lines are listed in Table 2. Additional details of our observing procedure and data analysis can be obtained from Kobayashi et al. (2007) and Kawakita & Kobayashi (2009).

3. Results

The gas production rates (Q, s^{-1}) were calculated from the observed spectra using modeled fluorescence efficiencies (g-factors) for the appropriate rotational excitation temperature (T_{rot}). Except for CH_3OH and C_2H_6, we used the g-factors derived from the fluorescence excitation models described in Kobayashi & Kawakita (2009).

Ro-vibrational lines from fundamental vibrational bands were observed for HCN, C_2H_2, CH_4, C_2H_6 and CH_3OH. These molecules are pumped from the ground vibrational state to the upper vibrational state by the solar radiation field and then relax down to the ground vibrational state. The population distribution among the rotational levels in the ground vibrational state is described by the Boltzmann distribution at a given rotational temperature T_{rot}.

Lines from the fundamental bands of H_2O cannot be detected by ground-based observations because of extinction from associated telluric lines. Instead, "hot-bands" are routinely observed from ground-based observatories (Dello Russo et al. 2004, 2005). The fluorescence excitation model of water hot-bands is based on Dello Russo et al. (2004, 2005); H_2O molecules are pumped from the ground vibrational state to the upper vibrational states by the solar radiation field and then cascade to the ground vibrational state through the intermediate vibrational states. The population distribution in the ground vibrational state is described by the Boltzmann distribution as for HCN, C_2H_2, CH_4, C_2H_6, and CH_3OH.

The detection of several lines of H_2O and HCN allows us to determine the rotational temperature T_{rot} of H_2O on Jan. 28 and Feb. 4 and of HCN on Jan. 28. We used the method outlined by Dello Russo et al. (2004). We plotted the ratios of line flux to the corresponding line g-factor (F/g) vs. the upper state rotational energy (E' – E'(lowest)) (Figure 4). At the appropriate T_{rot}, the slope of the line for F/g vs. (E' – E'(lowest)) should be equal to zero because at this temperature F/g should be independent of (E' – E'(lowest)).

We determined the best T_{rot} for H_2O by the χ^2-fitting method. Errors ($\pm 1\sigma$) in T_{rot} and the ortho-to-para ratio (OPR) are estimated based on the reduced χ^2. The T_{rot} of H_2O is determined to be 70 ± 15 K and $65\ ^{+15}_{-13}$ K for Jan. 28 and Feb. 4, respectively. The OPR for H_2O was also determined but it was poorly constrained. The best-fit values are $2.35^{+0.77}_{-0.58}$ and $2.56^{+1.50}_{-0.74}$ on Jan 28 and Feb 4, respectively. These values are consistent with the high-temperature limit (OPR = 3) within their uncertainties. Therefore, we assume OPR = 3 in the following part. For HCN, we determined T_{rot} = 54 ± 9 K on Jan. 28 (Figure 4). The $\pm 1\sigma$ uncertainty for the T_{rot} is estimated from the error in the slope. The rotational temperatures for H_2O and HCN on Jan. 28 are consistent within their uncertainties. The spatial profiles of H_2O and HCN are also shown in

Figure 4 and these profiles are consistent with each other. These facts suggest that the rotational excitation of these molecules was controlled by intermolecular collisions in the inner coma, so these molecules were thermalized. Therefore, we assumed a $T_{\rm rot}$ of 70 K on both Jan. 28 and Feb. 4 for molecules where rotational temperatures could not be directly determined (C_2H_2, CH_4, C_2H_6 and CH_3OH).

For C_2H_6, g-factors of detected lines were provided by Dello Russo et al. (2001) at $T_{\rm rot}$ = 70 K. We used those g-factors to determine the mixing ratio of C_2H_6. Usually, CH_3OH production rates from high-resolution infrared measurements are determined from the flux of the ν_3 Q-branch. However, the ν_3 Q-branch was observed when the comet was at high airmass ($\sim$ 2.5), so flux-calibration for this setting was more uncertain. Therefore, a CH_3OH production rate was determined from the flux of ν_2 lines detected near 3000 cm^{-1}. These same lines were detected in comet C/1999 H1 Lee along with the ν_3 Q-branch of CH_3OH, and fluxes for these lines were reported in Dello Russo et al. (2006). The gas rotational temperatures derived from C/1999 H1 Lee were between 70 and 80 K (Mumma et al. 2001a; Dello Russo et al. 2005), similar to the derived gas rotational temperatures reported here for 8P/Tuttle. Therefore, assuming the relative intensities of the ν_2 CH_3OH lines and the ν_3 Q-branch are the same in both comets, effective g-factors could be determined for the ν_2 CH_3OH lines using the modeled g-factor for the ν_3 Q-branch. We used the CH_3OH ν_3 Q-branch g-factor at 70 K used by Bonev et al. (2008) and Boehnhardt et al. (2008) to enable a direct comparison with their derived CH_3OH production rate (DiSanti, private comm.).

Gas production rates are determined based on the isotropic expanding coma model (e.g., Kobayashi et al. 2007). We assumed the expansion velocity of gas to be $0.8 \times r^{-0.5}$ km s^{-1} (r is the heliocentric distance of the comet in AU). Photodissociation rates of the molecules are taken from Huebner et al. (1992). In order to determine the absolute production rates, the "Q-curve" method (correction for the slit-loss of the comet) was used (DiSanti & Mumma 2008). We assumed that the "growth factor" (a ratio of the global Q relative to the nucleus-centered Q) is the same for all species observed at the same time. For example, we determined the growth factor of C_2H_6 from its emission lines and we applied it to CH_4 and CH_3OH (these emission lines were observed simultaneously) since the emission lines of both CH_4 and CH_3OH are too weak to determine the growth-factor based on their signals only. We determined the growth-factors of H_2O (January 28: 2.22 ; February 4: 2.55) and C_2H_6 (3.54) and we applied them to other molecules in each setting. On February 4, the growth-factor of C_2H_6 is 40 % higher than that of H_2O. This difference might be caused by the difference of seeing for these settings (seeing is much better on setting #1' than setting #3).

The mixing ratios of parent volatiles in 8P/Tuttle are determined as production rate ratios relative to H_2O (i.e., $Q(X)/Q(H_2O)$). For HCN and C_2H_2, we derived the mixing ratios by comparing directly their emission lines with H_2O lines (taken simultaneously, see Table 2). The growth factors are canceled in these cases. In other cases (CH_4, C_2H_6, and CH_3OH), the molecular emission lines were not observed with H_2O simultaneously and both the growth factors of H_2O and each molecular species are used to derive the mixing ratios. The uncertainties in production rates and mixing ratios are dominated by systematic uncertainty (e.g., accuracy of the fluorescence model for each molecule, accuracy of model calculation of the atmospheric transmittance etc.) and not generally by the stochastic noise mainly caused by sky-background emission. We employed the standard deviation of the F/g values as the systematic uncertainty. Production rates and mixing ratios for all detected molecules are listed in Table 3.

4. Discussion

Radar observations obtained by Harmon et al. (2008) suggest that the nucleus of 8P/Tuttle is a "contact binary" with a rotational period of 11.4 hours. Because of this, Bonev et al. (2008) hypothesized that the components of 8P/Tuttle might be chemically heterogeneous. Comparing mixing ratios obtained from our observations to those obtained from other high-resolution infrared observations carried out in December 2007 and January 2008 (Bonev et al. 2008; Boehnhardt et al. 2008) suggests no evidence for temporal variation of the coma composition in 8P/Tuttle (Table 4 and Figure 5) because these mixing ratios are consistent within three σ error-bars. This is confirmed by a χ^2 test of hypothsis which, even at the 0.01 significance level, does not allow us to reject the hypothesis of constant mixing ratios. We note that the emission lines used to determine the mixing ratio of CH_3OH in our analysis and in others (Bonev et al. 2008; Boehnhardt et al. 2008) were different i.e., the ν_2 lines in ours as listed in Table 2 and the ν_3 Q-branch in others. This implies that the error of g-factor we used may be larger because we converted the g-factor of the ν_3 Q-branch to ν_2 lines based on the observations of comet Lee for CH_3OH. Since we did not consider the error of the g-factor of the ν_3 Q-branch and the error for the conversion from the ν_3 Q-branch to the ν_2 lines, the error of CH_3OH mixing ratio might be larger.

The absolute production rate of water in late January is almost the same between our work on January 28 UT and Boehnhardt et al. (2008) on January 27 UT. Given the rotation period measured by Harmon et al. (2008) and Lamy et al. (2008), our observations of January 28 and February 4 were separated by $\approx$ 14.65 rotations, i.e., they were done at rotation phases separated by one third of the nucleus rotation period. The measurements of Boehnhardt et al. (2008) are at phases in between our measurements. Given the uncertainties in the rotation period of 8P/Tuttle, the rotation phase of the December observations (Bonev et al. 2008) cannot be properly scaled with respect to our measurements. If the nucleus had two components of significantly different chemical composition, as suggested by Bonev et al. (2008), variations of the coma composition should have been observed. Based on these near-IR measurements, there is no evidence for chemical heterogeneity within the nucleus of 8P/Tuttle.

We also compared the mixing ratios with other HFCs and LPCs listed in DiSanti & Mumma (2008), and summarized them in Table 5 and Figure 6. Although the black bars shown in Figure 6 indicate a wide range (by a factor of $\sim$10) of mixing ratios, most of this variation is caused by C/1999 S4 (LINEAR) and C/2001 A2 (LINEAR). The former is highly depleted in organic volatiles while the latter is rich in organics (see Table 5). From near-IR measurements of comets, some chemical groups are proposed by Mumma et al. (2009); organics-enriched, -normal, and

-depleted group. Comet C/1999 S4 (LINEAR) and C/2001 A2 (LINEAR) represent comets of the organics-depleted and the organics-enriched group, respectively. On the other hand, Crovisier et al. (2009) reported that there is no clear evidence of such grouping by chemistry in radio observations. The chemical taxonomy of comets is still under debate and the lack of samples makes this problem more complex. Therefore, we plotted the mixing ratios of comets without such a grouping, just as a range. In comparison to other HFCs (1P/Halley and 153P/Ikeya-Zhang), 8P/Tuttle is strongly depleted in C_2H_2 and may also be depleted in HCN and C_2H_6. On the other hand, in comparison to 6 LPCs, the mixing ratios in comet 8P/Tuttle are within the ranges typically seen, with HCN and C_2H_2 at the depleted end while CH_3OH is in the upper range.

A similar composition was also reported by Bonev et al. (2008). They suggested that the composition of 8P/Tuttle was unusual and that it might be caused by chemical heterogeneity in the nucleus if the binary components are chemically distinct. However, as we mentioned above, the mixing ratios of species in 8P/Tuttle are not atypical and there is no evidence of heterogeneity in chemistry by comparing the composition on different dates. Does the chemistry of 8P/Tuttle suggest a different formation region than the HFCs and LPCs? HFCs and LPCs are thought to have formed in the region from 5 – 30 AU in the early solar nebula. JFCs likely formed in a more compact region (16 – 30 AU) (Morbidelli et al. 2008). While 8P/Tuttle may have formed in a different region of the early solar nebula from other HFCs and LPCs, based on the derived volatile mixing ratios there is no conclusive evidence.

Bonev et al. (2008) reported that C_2H_6 might be formed from C_2H_2 by hydrogen atom addition reactions, and that this conversion may have occurred with higher efficiency in 8P/Tuttle than in typical OC comets. Our observations show no conclusive evidence for this hypothesis. From our detection of C_2H_2 we determined that the mixing ratio of C_2H_2 to H_2O is consistent with the upper-limit reported in Bonev et al. (2008). In order to test this hypothesis, we use the $C_2H_6/(C_2H_6+C_2H_2)$ ratio to estimate the conversion rate from C_2H_6 to C_2H_2. We compared the ratio obtained in 8P/Tuttle with other HFCs and LPCs listed in Table 5. Table 6 and Figure 7 show the $C_2H_6/(C_2H_6+C_2H_2)$ ratios in these different comets. The conversion efficiency from C_2H_2 to C_2H_6 in 8P/Tuttle is consistent with the values obtained in other HFCs and LPCs within the limitations of sample size (within the 99% confidence limit (hereafter, c.l.), see Figure 7).

Bonev et al. (2008) also reported that the mixing ratios of HCN and C_2H_2 are inconsistent with these species being the only native precursors of the CN and C_2 radicals observed at optical wavelengths. We computed $\log_{10}[Q(\mathrm{HCN})/Q(\mathrm{H_2O})]$, $\log_{10}[Q(\mathrm{C_2H_2})/Q(\mathrm{H_2O})]$ and $\log_{10}[Q(\mathrm{C_2H_2})/Q(\mathrm{HCN})]$ and compared our results with optical results (see Table 7), including a measurement of the C_2/CN ratio at a time coincident with our CRIRES observations (Jehin et al. 2009). Possible precursors of C_2 observed in the near infrared are C_2H_2 and C_2H_6. Although C_2H_6 is not a direct parent of C_2, it may contribute to its abundance. According to Helbert et al. (2005), C_2H_6 can photodissociate to C_2H_5 (∼33%) and C_2H_4 (∼37%). All C_2H_5 and a fraction of C_2H_4 (∼ 44%) photodissociate to C_2H_2. Finally, all of C_2H_2 is photodissociated to C_2. Based on this C_2 is formed from C_2H_6 at about 50 % yield (∼33% ($C_2H_6 \rightarrow C_2H_5 \rightarrow C_2H_2$) + ∼16% ($C_2H_6 \rightarrow C_2H_4 \rightarrow C_2H_2$)). We note that this is only an approximation as these branching ratios are uncertain and dependent on the wavelength of the irradiating photon (Helbert et al. 2005). Assuming the branching ratios are correct, the mixing ratio $\log_{10}[Q(\mathrm{C_2})/Q(\mathrm{OH})] \sim \log_{10}[(Q(\mathrm{C_2H_2}) + 0.5Q(\mathrm{C_2H_6}))/Q(\mathrm{H_2O})]$ if C_2H_2 and C_2H_6 are the primary parents of C_2. However, $\log_{10}[Q(\mathrm{C_2})/Q(\mathrm{OH})]$ is significantly larger than $\log_{10}[(Q(\mathrm{C_2H_2}) + 0.5Q(\mathrm{C_2H_6}))/Q(\mathrm{H_2O})]$, and this is true even assuming that C_2H_6 completely photodissociates to C_2. Our derived mixing ratio for HCN is also too low to explain the CN abundance in 8P/Tuttle (e.g., $\log_{10}[Q(\mathrm{CN})/Q(\mathrm{OH})] > \log_{10}[Q(\mathrm{HCN})/Q(\mathrm{H_2O})]$). A direct comparison of the HCN and CN production rates measured simultaneously at the VLT on January 28 yields CN/HCN ∼ 3 (Jehin et al. 2009). To explain the CN and C_2 abundances in 8P/Tuttle, at least one additional precursor of both CN and C_2 is needed. Our results agree with the conclusion of Bonev et al. (2008).

The discrepancy between gas production rates of parents and their daughter species was reviewed by Fray et al. (2003) for HCN and CN. They compared HCN and CN production rates in eight comets and they found that the CN production rates are significantly higher than those of HCN in four comets while the CN and HCN production rates are similar to each other in other comets. An additional process is required for the CN production other than HCN photolysis in the former case.

5. Summary and conclusion

We observed comet 8P/Tuttle on January 28 and February 4 with the ESO VLT. Our observations were carried out in multiple spectral regions (optical and near IR), with this paper focusing on high dispersion spectroscopic observations of near IR data obtained with CRIRES. We determined the rotational temperatures for H_2O and HCN, and the production rates and abundance ratios of several parent volatiles in 8P/Tuttle. We compared our results to other high dispersion near IR spectroscopic observations reported by Bonev et al. (2008) and Boehnhardt et al. (2008). Mixing ratios obtained from both studies are consistent with each other and we found no evidence of chemical heterogeneity from these observations. We also compared our results to those for other HFCs and LPCs. 8P/Tuttle is strongly depleted in C_2H_2 and may also be depleted in HCN and C_2H_6 relative to other HFCs. On the other hand, relative abundances of volatiles in 8P/Tuttle are not atypical when compared to LPCs, with C_2H_2 and HCN on the depleted end and CH_3OH slightly enhanced. Although it is possible that the formation region of 8P/Tuttle is different from the formation regions of other LPCs and HFCs, we note that diverse chemistry is also seen within the Oort cloud population. We determined conversion efficiencies for hydrogen atom addition reactions through the $C_2H_6/(C_2H_6+C_2H_2)$ ratio in 8P/Tuttle and other comets. We found that $C_2H_6/(C_2H_6+C_2H_2)$ in 8P/Tuttle is consistent with other LPCs and HFCs (99% c.l.) contrary to the high conversion efficiency reported by Bonev et al. (2008). However, we note that it is difficult to discern any trends as the number of comets where $C_2H_6/(C_2H_6+C_2H_2)$ ratios are measured is small. It is generally assumed that CN is formed directly from HCN and that C_2 is formed directly

from C_2H_2 and indirectly from C_2H_6 in cometary comae. However, Fray et al. (2003) reported a discrepancy between CN and HCN production rates in four comets (suggesting an additional process is required for the CN production). In the case of 8P/Tuttle the abundances of HCN, C_2H_2 and C_2H_6 are insufficient to explain the CN and C_2 abundances. So we concluded that at least one additional parent is needed for each species, as pointed out by Bonev et al. (2008).

Acknowledgements. The authors thank the anonymous referee for helpful comments. H. Kobayashi is JSPS fellow of the Ministry of Education, Science, Sports and Culture (Japan). EJ is Research Associate FNRS (Belgium), JM is Research Director FNRS and DH is Senior Research Associate FNRS.

References

A'Hearn, M. A., M. A., Mills, R. L., Schleicher, D. G., Osip, D. J., and Birch, P. V. 1995, Icarus, 118, 223
Biver, N., Bockelée-Morvan, D., Crovisier, J., Davies, J. K., Matthews, H. E., Wink, J. E., Rauer, H., Colom, P., Dent, W. R. F., Despois, D., Moreno, R., Paubert, G., Jewitt, D., Senay, M. 1999a, AJ, 118, 1850
Biver, N., Bockelée-Morvan, D., Colom, P., Crovisier, J., Germain, B., Lellouch, E., Davies, J. K., Dent, W. R. F., Moreno, R., Paubert, G., Wink, J., Despois, D., Lis, D. C., Mehringer, D., Benford, D., Gardner, M., Phillips, T. G., Gunnarsson, M., Rickman, H., Bergman, P., Johansson, L. E. B., Winnberg, A., Rauer, H. 1999b, Earth Moon and Planets, 78, 5
Biver, N., Bockelée-Morvan, D., Crovisier, J., Colom, P., Henry, F., Moreno, R., Paubert, G., Depois, D., Lis, D. C. 2002, Earth Moon and Planets, 90, 323
Bockelée-Morvan, D., Crovisier, J., Mumma, M. J., & Weaver, H. A. 2004, in Comets II, ed. Festou M., Keller, U. H., and Weaver, H. A. (the University of Arizona Press, Tucsom) 275
Bockelée-Morvan, D., Crovisier, J., Despois, D., Forveille, T., Gérard, E., Schraml, J., & Thum, C. 1987, A&A, 180, 253
Bonev, B. P., Mumma, M. J., Radeva, Y. L., DiSanti, M. A., Gibb, E. L., Villanueva, G. L. 2008, ApJ, 680, L61
Boehnhardt, H., Mumma, M. J., Villanueva, G. L., DiSnati, M. A., Bonev. B. P., Lippi, M., Käufl, H. U. 2008, ApJ, 683, L71
Clough, S. A., and Iacono, M. J. 1995, J. Geophys. Res., 100, 16519
Crovisier, J., Biver, N., Bockelée-Morvan, D., Boissier, J., Colom, P., 2008, SF2A-2008: Proceedings of the Annual meeting of the French Society of Astronomy and Astrophysics ed. C. Charbonnel, F. Combes and R. Samadi. Available online at http://proc.sf2a.asso.fr, 40
Crovisier, J., Biver, N., Bockelée-Morvan, D., Boissier, J., Colom, P., Lis D. C. 2009, Earth Moon and Planets, 105, 267
Dello Russo, N., Mumma, M. J., DiSanti, M. A., Magee-Sauer, K., Novak, R. 2001, Icarus, 153, 162
Dello Russo, N., DiSanti, M. A., Magee-Sauer, K., Gibb, E. L., Mumma, M. J. 2002a Asteroids, Comets, Meteors., ESA SP-500, ESTEC(Noordwijk), 689
Dello Russo, N., Mumma, M. J., DiSanti, M. A., Magee-Sauer, K. 2002b, J. Geophys. Res., 107(E11), 5095
Dello Russo, N., DiSanti, M. A., Magee-Sauer, K., Gibb, E. L., Mumma, M. J., Barber, R. J., Tennyson, J. 2004, Icarus, 168, 186
Dello Russo, N., Bonev, B. P., DiSanti, M. A., Mumma, M. J., Gibb, E. L., Magee-Sauer, K., Barber, R. J., Tennyson, J. 2005, ApJ, 621, 537
Dello Russo, N., Mumma, M. J., DiSanti, M. A., Magee-Sauer, K., Gibb, E. L., Bonev, B. P., McLean, I. S., Xu, Li-Hong. 2006, Icarus, 184, 255
Dello Russo, N., Verback, R. J., Weaver, H. A., Lisse, C. M. 2009, Icarus, 200, 271
Despois, D., Crovisier, J., Bockelée-Morvan, D., Schraml, J., Forveille, T., Gérard, E. 1986, A&A, 160, L11
DiSanti, M. A., Dello Russo, N., Magee-Sauer, K., Gibb, E. L., Reuter, D. C., Mumma, M. J. 2001, Asteroids, Comets, Meteors., ESA SP-500, ESTEC(Noordwijk), 571
DiSanti, M. A. and Mumma, M. J. 2008, Space Sci. Rev., 138, 127
Duncan, M. J. 2008, Space Sci. Rev., 138, 109
Eberhardt, P., Meier, R., Krankowsky, D., Hodges, R. R. 1994, A&A, 288, 315
Eberhardt, P. 1999, Space Sci. Rev., 90, 45
Fray, N., Bénilan, Y., Cottin, H., Gazeau, M.-C., Crovisier, J. 2003, Planet. Space Sci., 53, 1243
Gibb, E. L., Mumma, M. j., Dello Russo, N., DiSanti, M. A., Magee-Sauer, K. 2003, Icarus, 165, 319
Gibb, E. L., DiSanti, M. A., Magee-Sauer, K., Dello Russo, N., Bonev, B. P., Mumma, M. J. 2007, Icarus, 188, 224
Harmon, J. K., Nolan, M. C., Howell, E. S., Giorgini, J. D., Margi, C. 2008, Asteroids, Comets, Meteors., Abstract #8025, Lunar and Planetary Institute Contribution No 1405, Houston (CD-ROM)
Helbert, J., Rauer, H., Boice, D. C., Huebner, W. F. 2005, A&A, 442, 1107
Huebner, W. F., Keady, J. J., Lyon, S. P. 1992, Astrophys. and Sp. Sci., 195, 1
Jehin, E., Bockelée-Morvan, D., Dello Russo, N., Manfroid, J., Hutsemékers, D., Kawakita, H., Kobayashi, H., Schulz, R., Smette, A., Stüwe, J., Weiler, M., Arpigny, C., Biver, N., Cochran, A., Crovisier, J., Rauer, H., Verback, R., Weaver, H., Zucconi, J. -M. 2009, Earth Moon and Planets, 105, 343
Käufl, H-U. and 23 colleagues, 2004, SPIE, 5482, 1218
Kawakita, H. and Kobayashi, H. 2009, ApJ, 693, 388
Kobayashi, H. & Kawakita, H. 2009, ApJ, 703, 121
Kobayashi, H., Kawakita, H., Mumma, M. J., Bonev, B. P., Watanabe, J., and Fuse, T. 2007, ApJ, 668, L75
Lamy, P. L., Toth, I., Jorda, L., Weaver, H. A., Groussin, O., A'Hearn, M. F. 2008, DPS meeting, BAAS 40, 393
Levison, H. F. 1996, in ASP Conf. Ser. 107: Completing the Inventory of the Solar System, 173 ed. Retting, T. & Hahn, J. M.
Magee-Sauer, K., Mumma, M. J., DiSanti, M. A., Dello Russo, N., Retting, T. W. 1999, Icarus, 142, 498
Magee-Sauer, K., Mumma, M. J., DiSanti, M. A., Dello Russo. N. 2001, DPS meeting, BAAS 33. 1076
Magee-Sauer, K., Dello Russo. N., DiSanti, M. A., Gibb, E. L., Mumma, M. J. 2002a, Asteroids, Comets, Meteors., ESA SP-500, ESTEC(Noordwijk), 549
Magee-Sauer, K., Mumma, M. J., DiSanti, M. A., Dello Russo. N. 2002b, J. Geophys. Res., 107(E11), 5096
Magee-Sauer, K., Mumma, M. J., DiSanti, M. A., Dello Russo. N., Gibb, E. L., Bonev, B. P. 2008, Icarus, 194, 347
Morbidelli, A., Levison, H. F., Gomes, R. 2008, in The Solar System beyond Neptune, ed. M. A. Barucci et al. (the University of Arizona Press, Tucsom) 275
Mumma, M. J., DiSanti, M. A., Dello Russo, N., Fomenkova, M., Magee-Sauer, K., Kaminski, C. D., Xie, D. X. 1996, Science, 194, 347
Mumma, M. J., DiSanti, M. A., Bonev, B. P., Villanueva, G. L., Magee-Sauer, K. Gibb, E. L. 2009, Asteroids, Comets, Meteors., Abstract #8282, Lunar and Planetary Institute Contriution No 1450, Houston (CD-ROM)
Mumma, M. J., McLean, I. S., DiSanti, M. A., Larkin, J. E., Dello Russo, N., Magee-Sauer, K., Becklin, E. E., Bida, T., Chaffee, F., Conrad, A. R., Figer, D. F., Gilbert, A. M., Graham, J. R., Levenson, N. A., Novak, R. E., Reuter, D. C., Teplitz, H. I., Wilcox, M. K., Xu, L.-H. 2001a, ApJ, 546, 1183
Mumma, M. J., Dello Russo, N., DiSanti, M. A., Magee-Sauer, K., Novak, R. E., Brittain, S., Retting, T., McLean, Reuter, D. C., Xu, L.-H. 2001b, Sciene, 292, 1334
Schloerb, F. P., Kinzel, W. M., Swade, D. A., & Irvine, W. M. 1986, ApJ, 310, L55
Weaver, H. A., Brroke, T. Y., Chin, G., Kim, S. J., Bockelée-Morvan, D., Davies, J. K. 1999, Earth Moon and Planets, 78, 71

[1] Department of Physics, Faculty of Science, Kyoto Sangyo University, Motoyama, Kamigamo, Kita-ku, Kyoto, Japan
e-mail: h_kobayashi@cc.kyoto-su.ac.jp
[2] LESIA, Observatoire de Paris, 5 place Jules Janssen, F-92195 Meudon, France
[3] Space Department, The Johns Hopkins University Applied Physics Laboratory, 11100 Johns Hopkins Road, Laurel, MD 20723-6099, USA
[4] Institut d'Astrophysique et de Géophysique, Sart-Tilman, B-4000, Liège, Belgium,
[5] European Southern Observatory, Alonso de Cordova 3107, Vitacura, Santiago 19, Chile
[6] Leiden Observatory, NL-2300 RA Leiden, The Netherlands

[7] GEPI, Observatoire de Paris, 5 place Jules Janssen, F-92195 Meudon, France
[8] Department of Astronomy and McDonald Observatory, University of Texas at Austin, Austin, USA,
[9] ESA/RSSD, ESTEC, P.O. Box 299, NL-2200 AG Noordwijk, The Netherlands
[10] Observatoire de Besançon, F-25010 Besançon Cedex, France

Table 1. Overview of the CRIRES observations.

Date	Time[a] (UT)	Settings	Molecules	Wavelength coverage [cm^{-1}]	r[b] [AU]	Δ[c] [AU]	$\dot{\Delta}$[d] [km/s]	Airmass	Slit P.A. [deg]
January 28, 2008	1:28 – 2:47	#2	H_2O, HCN, C_2H_2	3332.4 – 3263.4	1.027	0.523	24.798	1.36	74
	3:13 – 4:07	#1	H_2O	3462.5 – 3377.0	1.027	0.524	24.865	2.03	74
February 4, 2008	0:49 – 1:54	#1'	H_2O	3406.2 – 3327.7	1.035	0.621	24.187	1.27	80
	2:20 – 3:23	#3	CH_4, CH_3OH, C_2H_6	3404.8 – 2974.2	1.035	0.622	24.252	1.69	80
	3:53 – 4:11	#4	CH_3OH	2865.3 – 2799.6	1.035	0.622	24.275	2.52	80

[a] r, Δ, and $\dot{\Delta}$ listed in column 6, 7, and 8 are the values at the midpoint of this time interval.
[b] heliocentric distance.
[c] geocentric distance.
[d] topocentric velocity of the comet.

Table 2. Line identification of detected emissions. Flux values listed in the 4th column are calibrated but not corrected for the telluric absorption. The g-factors listed in the 5th column are calculated for the observational conditions. Field of view of the aperture is 0.2" × ∼ 0.8". The *-mark indicates that the line is blended with the line above.

(a) January 28, 2008; H_2O

Transition $(\nu_1',\nu_2',\nu_3')J'_{K_a'K_c'}$ - $(\nu_1'',\nu_2'',\nu_3'')J''_{K_a''K_c''}$	Wavenumber [cm^{-1}]	Wavelength [Å]	Flux [W m^{-2}]	g-factor[(1)] [W $molecule^{-1}$]	atmospheric transmitta
$(101)1_{11}$-$(001)2_{02}$	3459.53	28905.67	$(8.60\pm1.27)\times10^{-20}$	2.48×10^{-27}	0.808
$(101)4_{31}$-$(100)5_{32}$	3459.49	28905.97	*	5.29×10^{-28}	0.809
$(101)4_{22}$-$(100)5_{23}$	3456.45	28931.44	$(3.90\pm1.08)\times10^{-20}$	4.29×10^{-27}	0.324
$(101)3_{03}$-$(001)3_{12}$	3455.43	28939.99	$(1.77\pm0.82)\times10^{-20}$	5.65×10^{-28}	0.814
$(101)2_{11}$-$(001)2_{20}$	3454.69	28946.17	$(9.28\pm0.81)\times10^{-20}$	3.70×10^{-27}	0.804
$(200)1_{10}$-$(001)2_{21}$	3453.30	28957.81	$(1.41\pm0.08)\times10^{-19}$	7.39×10^{-27}	0.795
$(101)2_{02}$-$(100)3_{21}$	3453.15	28959.03	$(1.34\pm0.09)\times10^{-19}$	5.62×10^{-27}	0.875
$(200)1_{10}$-$(001)1_{11}$	3450.29	28983.04	$(6.10\pm0.87)\times10^{-20}$	1.03×10^{-26}	0.214
$(110)3_{21}$-$(010)4_{32}$	3449.78	28987.36	$(2.50\pm0.77)\times10^{-20}$	6.46×10^{-28}	0.732
$(200)2_{20}$-$(001)2_{21}$	3445.89	29020.12	$(3.22\pm0.90)\times10^{-20}$	2.11×10^{-27}	0.490
$(200)2_{12}$-$(100)3_{21}$	3412.92	29300.39	$(1.10\pm0.08)\times10^{-19}$	4.68×10^{-27}	0.802
$(101)3_{13}$-$(001)4_{04}$	3411.62	29311.61	$(7.92\pm0.66)\times10^{-20}$	3.27×10^{-27}	0.940
$(201)1_{11}$-$(200)1_{10}$	3405.42	29364.95	$(5.98\pm0.72)\times10^{-20}$	1.78×10^{-27}	0.909
$(201)2_{21}$-$(200)2_{20}$	3405.39	29365.21	*	1.78×10^{-28}	0.896
$(101)1_{11}$-$(001)2_{21}$	3404.24	29375.11	$(3.82\pm0.77)\times10^{-20}$	1.65×10^{-27}	0.420
$(200)1_{11}$-$(001)2_{12}$	3403.23	29383.84	$(1.26\pm0.09)\times10^{-19}$	4.29×10^{-27}	0.758
$(200)1_{01}$-$(001)2_{02}$	3399.37	29417.23	$(4.01\pm0.08)\times10^{-19}$	1.36×10^{-26}	0.816
$(300)2_{12}$-$(101)1_{11}$	3389.14	29506.05	$(1.71\pm0.63)\times10^{-20}$	2.44×10^{-28}	0.936
$(201)0_{00}$-$(200)1_{01}$	3388.77	29509.23	$(8.34\pm0.66)\times10^{-20}$	2.65×10^{-27}	0.938
$(101)4_{04}$-$(001)5_{15}$	3387.54	29519.94	$(4.28\pm0.78)\times10^{-20}$	1.47×10^{-27}	0.891
$(201)2_{11}$-$(101)2_{02}$	3385.14	29540.66	$(2.62\pm0.94)\times10^{-20}$	7.16×10^{-29}	0.580
$(101)2_{11}$-$(001)3_{22}$	3385.14	29540.90	*	1.60×10^{-27}	0.563
$(200)2_{12}$-$(001)3_{13}$	3382.10	29567.43	$(3.79\pm0.07)\times10^{-19}$	1.22×10^{-26}	0.892
$(200)2_{02}$-$(001)3_{03}$	3378.48	29599.08	$(9.53\pm0.76)\times10^{-20}$	3.16×10^{-27}	0.746
$(101)3_{13}$-$(100)4_{22}$[(2)]	3320.13	30119.34	$(6.44\pm0.75)\times10^{-20}$	1.38×10^{-27}	0.966
$(200)3_{13}$-$(001)4_{22}$[(2)]	3319.47	30125.29	$(5.06\pm0.71)\times10^{-20}$	5.10×10^{-28}	0.968
$(101)3_{22}$-$(100)4_{31}$[(2)]	3319.12	30128.50	$(2.79\pm0.57)\times10^{-20}$	1.21×10^{-27}	0.959
$(101)4_{22}$-$(001)5_{33}$[(2)]	3308.06	30229.17	$(2.63\pm0.82)\times10^{-20}$	7.46×10^{-28}	0.678

(1) $T_{\rm rot}$ = 70 K., (2) In setting #2

(b) January 28, 2008; HCN ν_3-band

Transition	Wavenumber [cm^{-1}]	Wavelength [Å]	Flux [W m^{-2}]	g-factor[(3)] [W $molecule^{-1}$]	atmospheric transmittance
R6	3331.59	30015.74	$(5.08\pm1.01)\times10^{-20}$	7.24×10^{-25}	0.97
R5	3328.78	30041.07	$(4.22\pm0.58)\times10^{-20}$	1.02×10^{-24}	0.94
R4	3325.94	30066.64	$(5.77\pm1.37)\times10^{-20}$	1.33×10^{-24}	0.90
R3	3323.09	30092.47	$(2.68\pm0.71)\times10^{-20}$	1.53×10^{-24}	0.59
R2	3320.22	30118.48	$(4.71\pm0.62)\times10^{-20}$	1.54×10^{-24}	0.97
R1	3317.33	30144.74	$(3.43\pm2.16)\times10^{-20}$	1.27×10^{-24}	0.86
P2	3305.54	30252.21	$(7.12\pm0.73)\times10^{-20}$	1.45×10^{-24}	0.96
P3	3302.55	30279.21	$(7.85\pm0.89)\times10^{-20}$	1.89×10^{-24}	0.96
P4	3299.53	30307.37	$(7.40\pm0.81)\times10^{-20}$	2.02×10^{-24}	0.93
P7	3290.35	30391.91	$(3.20\pm0.78)\times10^{-20}$	1.16×10^{-24}	0.90
P8	3287.25	30420.58	$(2.90\pm0.70)\times10^{-20}$	8.01×10^{-25}	0.95

(3) $T_{\rm rot}$ = 54 K.

Table 2. (continued).

(c) January 28, 2008; C_2H_2 ν_3-band

Transition	Wavenumber [cm^{-1}]	Wavelength [Å]	Flux [W m^{-2}]	g-factor[(4)] [W $molecule^{-1}$]	atmospheric transmittance
R3	3304.17	30267.30	$(1.73\pm0.61)\times10^{-20}$	1.03×10^{-24}	0.95
P3	3287.76	30418.40	$(3.22\pm0.82)\times10^{-20}$	1.05×10^{-24}	0.92
P5	3282.99	30462.99	$(2.25\pm0.89)\times10^{-20}$	1.27×10^{-24}	0.71

(4) $T_{\rm rot}$ = 70 K is assumed.

(d) February 4, 2008; H_2O

Transition $(\nu_1',\nu_2',\nu_3')J'_{K_a'K_c'}$ - $(\nu_1'',\nu_2'',\nu_3'')J''_{K_a''K_c''}$	Wavenumber [cm^{-1}]	Wavelength [Å]	Flux [W m^{-2}]	g-factor[(5)] [W $molecule^{-1}$]	atmospheric transmitta
$(201)1_{11}$-$(200)1_{10}$	3405.42	29364.95	$(4.07\pm0.78)\times10^{-20}$	1.81×10^{-27}	0.847
$(201)2_{21}$-$(200)2_{20}$	3405.39	29365.21	*	1.58×10^{-28}	0.822
$(200)1_{11}$-$(001)2_{12}$	3403.23	29383.84	$(6.84\pm0.77)\times10^{-20}$	4.63×10^{-27}	0.640
$(200)1_{01}$-$(001)2_{02}$	3399.37	29417.23	$(1.98\pm0.06)\times10^{-19}$	1.37×10^{-26}	0.738
$(200)2_{21}$-$(100)3_{30}$	3394.08	29463.10	$(1.00\pm0.06)\times10^{-19}$	1.10×10^{-26}	0.631
$(200)4_{14}$-$(001)4_{13}$	3390.04	29498.19	$(3.25\pm0.62)\times10^{-20}$	2.08×10^{-28}	0.738
$(101)2_{12}$-$(100)3_{31}$	3390.02	29498.38	*	1.47×10^{-27}	0.785
$(201)0_{00}$-$(200)1_{01}$	3388.77	29509.23	$(3.68\pm0.72)\times10^{-20}$	2.81×10^{-27}	0.900
$(200)2_{12}$-$(001)3_{13}$	3382.10	29567.43	$(1.63\pm0.05)\times10^{-19}$	1.25×10^{-26}	0.857
$(200)2_{02}$-$(001)3_{03}$	3378.48	29599.08	$(3.81\pm0.53)\times10^{-20}$	3.09×10^{-27}	0.770
$(200)2_{21}$-$(001)3_{22}$	3372.76	29649.35	$(9.25\pm0.53)\times10^{-20}$	7.13×10^{-27}	0.893
$(210)2_{21}$-$(110)3_{30}$	3361.03	29752.74	$(2.45\pm0.55)\times10^{-20}$	5.19×10^{-28}	0.656
$(200)3_{13}$-$(001)4_{14}$	3360.99	29753.14	*	1.77×10^{-27}	0.617
$(200)3_{03}$-$(001)4_{04}$	3358.92	29771.45	$(8.64\pm0.61)\times10^{-20}$	4.83×10^{-27}	0.783
$(201)2_{02}$-$(200)3_{03}$	3346.99	29877.58	$(6.73\pm0.63)\times10^{-20}$	2.60×10^{-27}	0.935
$(200)3_{12}$-$(001)4_{13}$	3341.17	29929.64	$(2.94\pm0.54)\times10^{-20}$	2.22×10^{-27}	0.899
$(200)4_{14}$-$(001)5_{15}$	3340.95	29931.63	$(2.71\pm0.53)\times10^{-20}$	2.13×10^{-27}	0.876
$(201)3_{13}$-$(200)4_{14}$	3329.42	30035.28	$(1.89\pm0.66)\times10^{-20}$	1.07×10^{-27}	0.847

(5) $T_{\rm rot}$ = 65 K.

(e) February 4, 2008; CH_4 ν_3-band

Transition	Wavenumber [cm^{-1}]	Wavelength [Å]	Flux [W m^{-2}]	g-factor[(6)] [W $molecule^{-1}$]	atmospheric transmittance
R1	3038.50	32913.67	$(2.03\pm0.78)\times10^{-20}$	1.20×10^{-24}	0.32
R0	3028.75	33019.58	$(3.44\pm0.76)\times10^{-20}$	1.46×10^{-24}	0.27

(6) $T_{\rm rot}$ = 70 K is assumed.

(f) February 4, 2008; C_2H_6 ν_7-band

Transition	Wavenumber [cm^{-1}]	Wavelength [Å]	Flux [W m^{-2}]	g-factor[(7)] [W $molecule^{-1}$]	atmospheric transmittance
$^RQ_0$	2986.73	33481.43	$(4.23\pm0.60)\times10^{-20}$	2.10×10^{-24}	0.91
$^PQ_1$	2983.38	33519.03	$(4.51\pm0.60)\times10^{-20}$	1.89×10^{-24}	0.94
$^PQ_2$	2980.07	33556.26	$(5.01\pm1.01)\times10^{-20}$	1.71×10^{-24}	0.79
$^PQ_3$	2976.77	33593.46	$(2.58\pm0.71)\times10^{-20}$	1.22×10^{-24}	0.91

(7) $T_{\rm rot}$=70 K is assumed, Dello Russo et al. (2001).

Table 2. (continued).

(g) February 4, 2008; CH_3OH ν_2-band

Transition	Wavenumber [cm^{-1}]	Wavelength [Å]	Flux [W m^{-2}]	g-factor[(8)] [W $molecule^{-1}$]	atmospheric transmittance
	3001.10	33323.83	$(4.80\pm0.88)\times10^{-20}$	2.86×10^{-25}	0.95
	3001.04	33324.49	*		0.94
	2997.16	33367.63	$(5.38\pm0.70)\times10^{-20}$		0.89
	2997.15	33367.75	*		0.85

(8) the g-factor of the ν_2 methanol line listed here is derived from the g-factor of the methanol ν_3-band Q-branch by comparing the intensities of these lines in cometary spectra (see text). The g-factor of the methanol ν_3-band Q-branch is taken equal to 5.80 $\times$ 10^{-25} [W/molecule] at $T_{\rm rot}$ = 70 K (DiSanti, private comm.).

Table 3. Production rates and mixing ratios of comet 8P/Tuttle.

January 28, 2008

Molecules	$T_{\rm rot}$ [K]	Production rate [molecules s^{-1}]	Mixing ratio [%]
H_2O	70±15	$(4.6\pm0.4)\times10^{28}$	100
HCN	54±9	$(3.4\pm1.1)\times10^{25}$	0.07±0.02
C_2H_2	(70)*	$(2.1\pm0.7)\times10^{25}$	0.05±0.02

February 4, 2008

Molecules	$T_{\rm rot}$ [K]	Production rate [molecules s^{-1}]	Mixing ratio [%]
H_2O	65^{+15}_{-13}	$(3.0\pm0.2)\times10^{28}$	100
CH_4	(70)*	$(1.7\pm1.1)\times10^{26}$	0.6±0.4
C_2H_6	(70)*	$(6.7\pm1.3)\times10^{25}$	0.23±0.04
CH_3OH	(70)*	$(9.7\pm1.3)\times10^{26}$	3.3±0.4

* This value is adopted, and is based on H_2O measurements (see text).

Table 4. Mixing ratios in comet 8P/Tuttle.

Molecules	This work	Bonev et al. (2008)	Boehnhardt et al. (2008)
HCN	0.07±0.02	0.07±0.02	
C_2H_2	0.05±0.02	<0.04	
CH_4	0.6±0.4	0.37±0.07	0.36±0.09/0.37±0.08(1)
C_2H_6	0.23±0.04	0.24±0.03	0.30±0.09/0.28±0.06(1)
CH_3OH	3.3±0.4	2.18±0.07	3.36±0.40/3.24±0.32(2)

(1) Measurements of January 26/27.
(2) Measurements of January 27/28.

Table 5. Mixing ratios of comet 8P/Tuttle, other HFCs and LPCs.

Comets	HCN	C_2H_2	CH_4	C_2H_6	CH_3OH	Remarks
8P/Tuttle	0.07±0.02	0.05±0.02	0.6±0.4	0.23±0.04	3.3±0.4	HFC, This work
153P/Ikeya-Zhang	0.18±0.05(1)	0.18±0.05(1)	0.51±0.06(2)	0.62±0.18(3)	2.5±0.5 (4)	HFC
1P/Halley	∼0.08-0.16(5,6,7)	∼0.3(8)	<1(8)	∼0.4(8)	1.7±0.4 (9)	HFC
C/1996 B2	0.18±0.04(10)	0.16±0.08(11)	0.79±0.08(2,12)	0.62±0.07(9,13)	1.7±0.4 (14)	LPC
C/1995 O1	0.27±0.04(11)	0.31±0.1(11)	1.45±0.16(2,15)	0.56±0.049(16)	2.4±0.3 (17)	LPC
C/1999 H1	0.29±0.02(18)	0.27±0.03(18)	1.45±0.18(2)	0.67±0.07(18)	2.1±0.5 (18)	LPC
C/2001 A2	0.6±0.01(19)	0.5±0.1(19)	1.2±0.2(20)	0.5±0.1(19)	3.9±0.4 (19)	LPC
C/1999 S4	0.10±0.03(21)	<0.12(21)	0.18±0.06(2,21)	<0.12(21)	<0.15(21)	LPC
C/2004 Q2	0.16±0.01(22)	0.054±0.004(22)	1.0±0.1(22)	0.42±0.01(22)	2.7±0.1 (22)	LPC

HFC : Halley Family Comet, LPC : Long Period Comet

(1)Magee-Sauer et al. (2002a), (2)Gibb et al. (2003), (3)Dello Russo et al. (2002a), (4)DiSanti et al. (2002), (5)Bockelée-Morvan et al. (1987), (6)Schloerb et al. (1986), (7)Despois et al. (1986), (8)Eberhardt (1999), (9)Eberhardt et al. (1994), (10)Magee-Sauer et al. (2002b), (11)Magee-Sauer et al. (2001), (12)Mumma et al. (1996), (13)Dello Russo et al. (2002b), (14)Biver et al. (1999a), (15)Weaver et al. (1999), (16)Dello Russo et al. (2001), (17)Biver et al. (1999b), (18)Mumma et al. (2001a), (19)Magee-Sauer et al. (2008), (20)Gibb et al. (2007), (21)Mumma et al. (2001b), (22)Kobayashi & Kawakita (2009)
[For CH_3OH, the same g-factor is used as Bonev's and Boehnhardt's. Mixing ratio listed here is higher by a factor of two than the reported value in their original paper (see, Kobayashi & Kawakita (2009)).]

Table 6. $C_2H_6/(C_2H_6+C_2H_2)$ ratios in comets.

Comets	$C_2H_6/(C_2H_6+C_2H_2)$ ratios	Remarks
8P/Tuttle	0.8±0.2	This work
153P/Ikeya-Zhang	0.8±0.4	DiSanti & Mumma (2008)
1P/Halley	∼0.6	DiSanti & Mumma (2008)
C/1996 B2	0.8±0.4	DiSanti & Mumma (2008)
C/1995 O1	0.6±0.2	DiSanti & Mumma (2008)
C/1999 H1	0.7±0.1	DiSanti & Mumma (2008)
C/2001 A2	0.8±0.1	DiSanti & Mumma (2008)
C/1999 S4	>0.5	DiSanti & Mumma (2008)
C/2004 Q2	0.9±0.1	Kobayashi & Kawakita (2009)
C/2006 P1	0.5±0.1	Dello Russo et al. (2009)

Table 7. HCN/H_2O (CN/OH), C_2H_2/H_2O (C_2/OH), and C_2H_2/HCN (C_2/CN) ratios in comet 8P/Tuttle.

$\log_{10}[\frac{Q(CN)}{Q(OH)}]$	$\log_{10}[\frac{Q(C_2)}{Q(OH)}]$	$\log_{10}[\frac{Q(C_2)}{Q(CN)}]$		Remarks
-2.54	-2.39	0.15		1980
-2.58	-2.41	0.17		2007
		0.11 - 0.15		2008, Jehin et al. (2009)
$\log_{10}[\frac{Q(HCN)}{Q(H_2O)}]$	$\log_{10}[\frac{Q(C_2H_2)}{Q(H_2O)}]$	$\log_{10}[\frac{Q(C_2H_2)}{Q(HCN)}]$	$\log_{10}[\frac{Q(C_2H_2+C_2H_6(50\%))}{Q(HCN)}]$	Remarks
$-3.13^{+0.11}_{-0.15}$	$-3.35^{+0.13}_{-0.17}$	$-0.22^{+0.17}_{-0.26}$	$0.33^{+0.13}_{-0.18}$	This work
$-3.14^{+0.04}_{-0.08}$	< -3.41	< -0.26		Bonev et al. (2008)

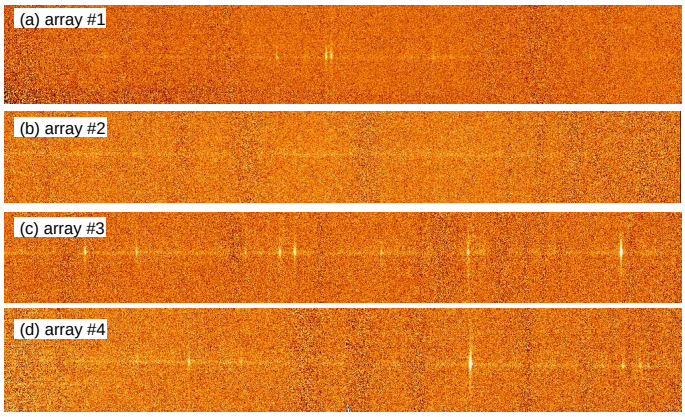

Fig. 1. Examples of two-dimensional spectra of comet 8P/Tuttle. Spectra shown in figures (a), (b), (c), and (d) were taken simultaneously by the four CRIRES arrays on January 28, 2008 using setting #1 (Table 1).

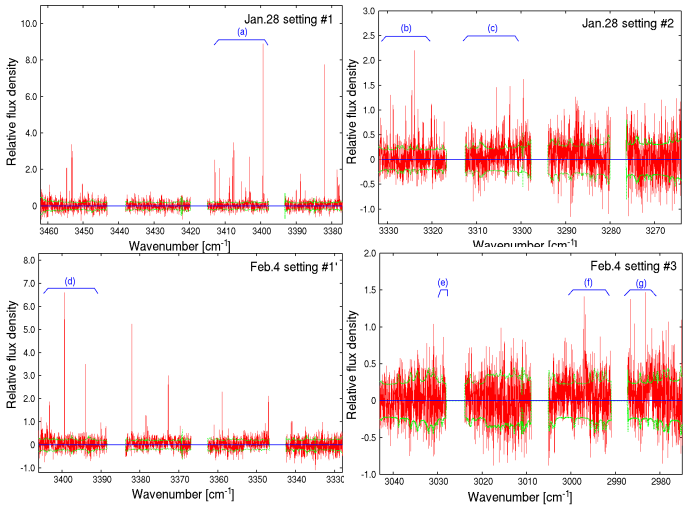

Fig. 2. Spectra of comet 8P/Tuttle. Each panel corresponds to each grating setting on each date. Part of spectra indicated by (a) — (g) are also shown in Figure 3 for more detail. Solid lines and dashed lines are zero levels and $\pm 1\sigma$ error levels, respectively in all panels. The field of view of the aperture is 0.2" $\times \sim$ 0.8".

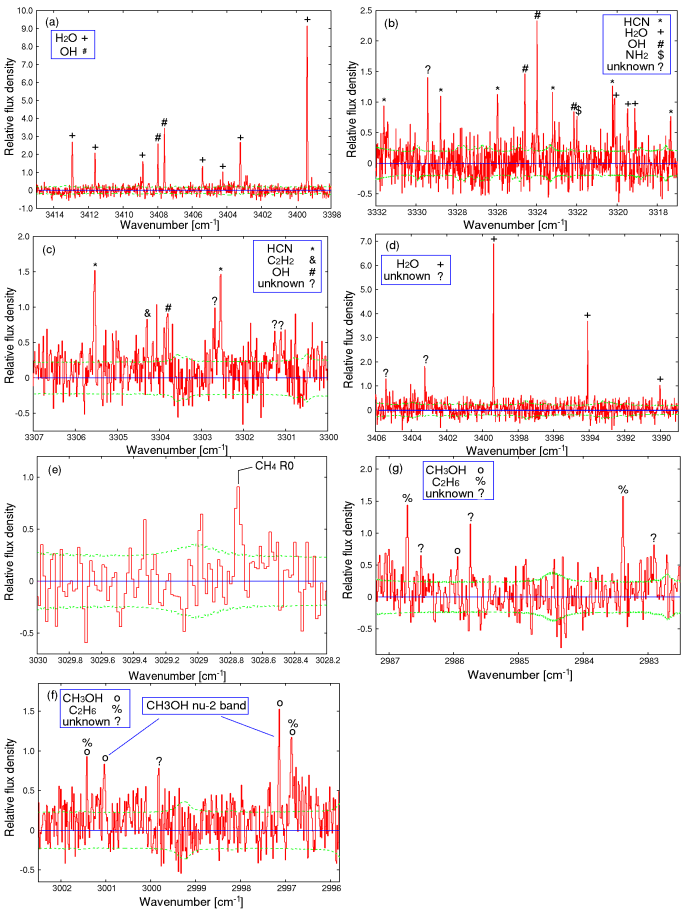

Fig. 3. Selected spectra of comet 8P/Tuttle. (a) Spectrum of H_2O and OH observed on January 28, 2008 (setting #1, see Table 1). (b) and (c) Spectra of HCN and C_2H_2 observed on January 28, 2008 (setting #2). (d) Spectrum of H_2O observed on February 4, 2008 (setting #1').(e),(f) and (g) Spectrum with CH_4 ν_3 R0 line, the ν_2 band of CH_3OH and the ν_7 band of C_2H_6 observed on February 4, 2008 (setting #3). Solid lines and dashed lines are zero levels and $\pm 1\sigma$ error levels, respectively in all panels. The field of view of the aperture is 0.2" $\times \sim$ 0.8".

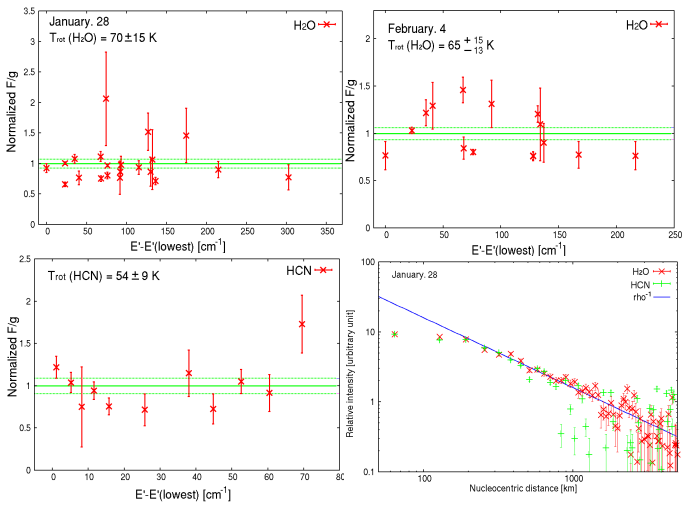

Fig. 4. Rotational temperature analysis of H_2O (on January 28 and February 4, 2008) and HCN (on January 28, 2008), and spatial profiles of H_2O and HCN (lower-right panel). For the rotatinal temperature analysis, we plot F/g vs. E'-E'(lowest) (upper state energy), where F is the line flux and g is the line g-factor. If the rotational temperature ($T_{\rm rot}$) used to compute the g-factors is correct, the line fitted to the F/g values should be flat. The inferred $T_{\rm rot}$ of H_2O is 70 ± 15 K and 65^{+15}_{-13} K on January 28 and February 4, respectively. $T_{\rm rot}$ of HCN is determined as 54 ± 9 K. The solid lines in the plots are the averaged F/g values (because F/g is normalized by the averaged F/g, the averaged F/g is unity). The errors-bars of $T_{\rm rot}$ and dashed lines in the figures correspond to $\pm1\sigma$ errors. For spatial profiles, the solid blue line corresnoinds to ρ^{-1} profile (ρ : nucleocentric distance), and the error-bars correspond to $\pm1\sigma$ errors for each data point.

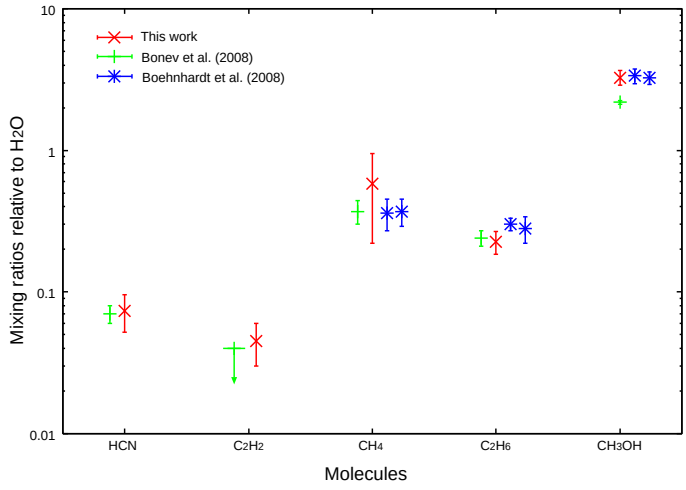

Fig. 5. Comparison of mixing ratios in comet 8P/Tuttle measured at different dates (this work, Bonev et al. (2008), and Boehnhardt et al. (2008), see Table 4). All error-bars are $\pm1\sigma$ error levels.

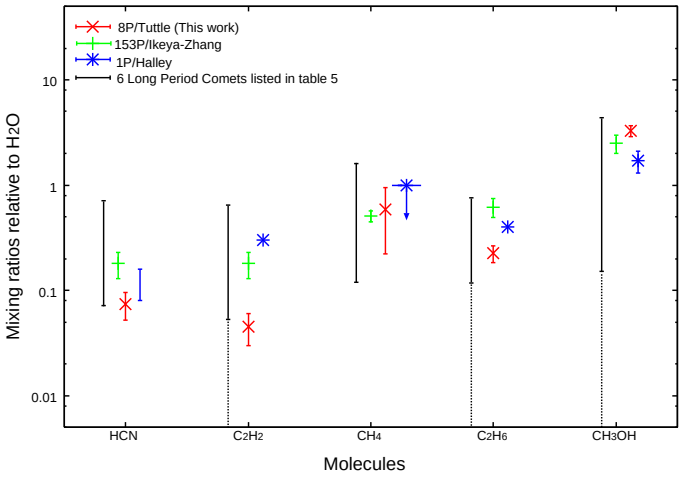

Fig. 6. Comparison between mixing ratios measured in 8P/Tuttle (this work) and in other Halley Family comets and 6 Long Period comets (DiSanti and Mumma, 2008, see Table 5). The black solid lines are the range of 6 Long Period comets. For the C_2H_2, C_2H_6, and CH_3OH of C/1999 S4 (LINEAR) is derived the upper limit (these molecules are shown as the ranges with the dashed lines below solid lines). Although all mixing ratios are within the range for 6 LPCs, HCN and C_2H_2 are at the lower end of each range. In contrast, CH_3OH is at the higher end of the range. All error bars are $\pm1\sigma$ error levels. Note that there are no reported error bars for some molecular species in the case of comet 1P/Halley (HCN, C_2H_2, and C_2H_6). For the HCN in comet 1P/Halley we show the range reported in some reports (see the references in Table 5).

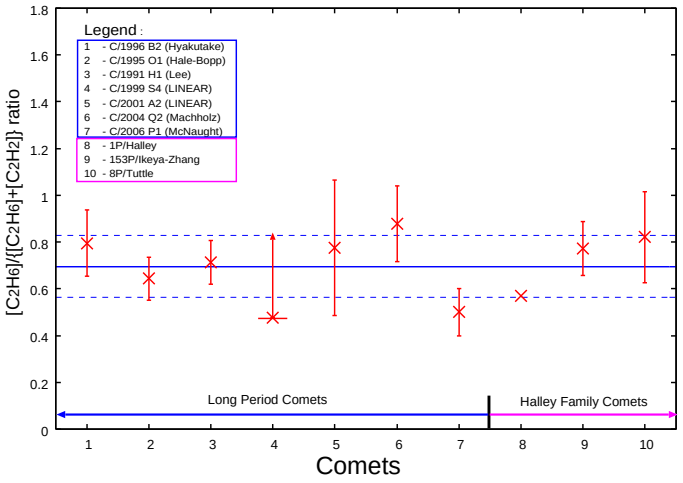

Fig. 7. The $C_2H_6/(C_2H_2+C_2H_6)$ ratio in comets listed in Table 6. The $C_2H_6/(C_2H_2+C_2H_6)$ ratio is considered as the conversion rate from C_2H_2 to C_2H_6 by hydrogen-addition reactions on cold grains in the solar nebula (or in the molecular cloud). All comets show similar conversion rates. The solid line shows the mean value of the $C_2H_6/(C_2H_2+C_2H_6)$ ratio and dashed lines show the $\pm1\sigma$ error levels of the $C_2H_6/(C_2H_2+C_2H_6)$ ratio. All error-bars are $\pm1\sigma$ error levels.